RSC Advances

ROYAL SOCIETY OF CHEMISTRY

www.rsc.org/advances

Insights into the Catalytic Mechanism of Chlorophenol 4-Monooxygenase: A Quantum Mechanics/Molecular Mechanics Study

Yanwei Li[†], Ruiming Zhang[†], Likai Du[‡], Qingzhu Zhang[†*], Wenxing Wang[†]

[†]Environment Research Institute, Shandong University, Jinan 250100, P. R. China

[‡]Key Laboratory of Bio-based Materials, Qingdao Institute of Bio-energy and Bioprocess Technology, Chinese Academy of Sciences, Qingdao 266101, P. R. China

Keywords

Catalytic mechanism, Polychlorinated phenols, Electrostatic influence, Quantum mechanical/molecular mechanical method

---

[*]Corresponding authors. E-mail: zqz@sdu.edu.cn

Fax: 86-531-8836 1990

Abstract

The catalytic mechanism of Chlorophenol 4-monooxygenase (TftD) toward substrate 2,4,5-trichlorophenol (2,4,5-TCP), 2,4,6-trichlorophenol (2,4,6-TCP), and 2,5-dichloro-p-hydroquinone (2,5-DiCHQ) were studied by quantum mechanical/molecular mechanical (QM/MM) investigations. The hydroxylation rather than dechlorination was found to be the rate determining step for all the three substrates. Substantial energy barrier spreads on the hydroxylation steps have been found. The corresponding Boltzmann-weighted average barriers are 16.3, 17.8, and 19.7 kcal mol^{-1} for 2,4,5-TCP, 2,4,6-TCP, and 2,5-DiCHQ, in accordance with the experimentally determined reaction rates. A previously unnoticed residue Arg100 was found to be important during the hydroxylation steps. Electrostatic influences of ten active site residues on the hydroxylation step were also investigated. Glu251 and Arg366 were highlighted as candidate residues for future mutation studies. In addition, we have shown that spatial location of 2,6-DiCHQ as well as the hydroxylation barrier are the two possible reasons why 2,6-DiCHQ cannot be further degraded by TftD.

1. Introduction

Chlorinated phenols (CPs) have been worldwide used as herbicides, preservatives, bactericides, fungicides as well as intermediates in the production of dyes or pharmaceuticals (*1*). The widespread distribution of CPs in the environment has caused serious concerns, mainly due to its toxicity, environmental persistence, and bioaccumulation properties (*2*). In addition, CPs can be transformed to carcinogenic chlorinated dibenzo-p-dioxins or dibenzofurans either though manufacturing processes or by means of biotransformation in soils (*3-5*). It is thus critically desiderated to set up strategies to minimize the continued exposure of these bio-accumulative pollutants to humans. Environmental biotransformation, one of the most promising strategies with the lowest power input, has provided some encouraging results and received worldwide acceptance in dealing with CPs (*1, 6-7*). Eighteen CPs are divided into five different groups based on the number of substituted chlorine atoms, such as mono-CPs (MCPs), di-CPs (DCPs), tri-CPs (TCPs), tetra-CPs (TeCPs), and penta-CPs (PCPs). Particularly, more attention has been focused on the bio-degradation of poly-CPs rather than MCPs, mainly due to its more recalcitrant character toward degradation (*8*).

Many bacteria have been found to be able to degrade poly-CPs, such as *Pseudomonas sp.* DP-4, *Rhodococcus erythropolis*, *Burkholderia cepacia* AC1100 (also known as *Burkholderia phenoliruptrix* AC1100), and *Mycobacterium chlorophenolicum* PCP-1 (*9-11*). Of all these bacteria, *Burkholderia cepacia* AC1100 has gained the most interest, partly due to its ability of using

2,4,5-trichlorophenoxyacetic acid as the sole carbon source, and partly due to its broad substrate specificity toward poly-CPs (*12-15*). *Burkholderia cepacia* AC1100 can efficiently degrade many poly-CPs, such as 2,4,5-trichlorophenol (2,4,5-TCP), 2,4,6-trichlorophenol (2,4,6-TCP), 2,3,4,6-trichlorophenol (2,3,4,6-TeCP), and pentachlorophenol (PCP) (*6, 16-17*). It has been validated that chlorophenol 4-monooxygenase (TftD) encoded by gene *tft*D is responsible for the degradation of poly-CPs (*18*).

Recent crystallization data (resolution 2.0 Å) has highlighted the composition of the active site residues of TftD at molecular level (*19*). Although co-crystalize of TftD-2,4,5-TCP or TftD-2,4,6-TCP complexes were not successful, the crystal structure shed light on understanding the degradation mechanism of TftD toward these poly-CPs. Combined with kinetic results, Xun and coworkers have been successfully proved that TftD firstly transforms 2,4,5-TCP to 2,5-dicholoro-p-benzoquinone (2,5-DiCBQ) in the presence of coenzyme flavin adenine dinucleotide ($FADH_2$), and then ejects 2,5-DiCBQ from the active site of TftD to the solution where 2,5-DiCBQ is transformed to 2,5-dichloro-p-hydroquinone (2,5-DiCHQ). After that, 2,5-DiCHQ can be re-utilized and degraded to 5-chloro-2-hydroxy-p-benzoquinone (5-Cl-2-H-BQ) by TftD. Finally, 5-Cl-2-H-BQ was transferred to 5-chloro-2-hydroxy-p-hydroquinone (5-Cl-2-H-HQ) in the solution environment (*16-19*) (Scheme 1). Similarly, TftD can transform 2,4,6-TCP to 2,6-dicholoro-p-benzoquinone (2,6-DiCBQ), and 2,6-DiCBQ is then transformed to 2,6-dichloro-p-hydroquinone (2,6-DiCHQ) in the solution. However, astonishingly,

no catalytic ability of TftD toward 2,6-DiCHQ was found (*14-15, 17, 19*).

Although the sequential degradation steps of TftD towards 2,4,5-TCP and 2,4,6-TCP have been established, an in-depth understanding of the corresponding elementary reactions for each step is still not available, mainly due to the limitations of the experimental facilities. For instance, co-crystalize of the reactant, intermediate, and product structures of TftD-$FADH_2$-2,4,5-TCP ternary complex were not successful. This obstructs our understanding on the catalytic machinery differences of diverse poly-CPs like 2,4,5-TCP and 2,4,6-TCP. In addition, mutation of His289 to Ala289 exhibits a dramatically decreased catalytic efficiency of TftD, which highlights a positive influence of His289 on the degradation processes (*19*). However, the roles of many other active site residues during the catalytic process of TftD were not elucidated. Understanding the roles of active site residues may provide valuable insights in further mutation studies, and can subsequently enhance enzyme activity toward poly-CP_S. In the present work, the detailed degradation processes of TftD toward 2,4,5-TCP, 2,5-DiCHQ, and 2,4,6-TCP have been investigated with the aid of a combined quantum mechanics/molecular mechanics (QM/MM) method. QM/MM calculations of the enzyme-catalyzed reaction can provide the atomistic details of the enzyme mechanism and are therefore becoming increasingly important to complement experimental enzyme chemistry (*20-22*). In order to better elucidate why TftD cannot degrade 2,6-DiCHQ, the catalytic mechanism of TftD toward 2,6-DiCHQ was also investigated in this study. In addition, a detailed study of the electrostatic influence of ten active site residues on the catalytic processes of TftD

toward 2,4,5-TCP, 2,4,6-TCP, and 2,5-DiCHQ have been performed.

2. Methods

2.1 Model preparation and molecular dynamics

The initial models for the present simulation were built on the basis of X-ray crystal structure of TftD (PDB code: 3HWC) obtained from Protein Data Bank (http://www.pdb.org). The protonation state of ionozable residues were determined on the basis of the pK_a values obtained via the PROPKA procedure and were manually verified through visual inspection (*23*). Missing hydrogen atoms in the crystal structure were added by using HBUILD facility in the CHARMM package (*24-26*). Since co-crystalize of $FADH_2$ and substrate (2,4,5-TCP or 2,4,6-TCP) with TftD were not successful, the configuration of FADHOOH (oxidation state of $FADH_2$) and substrate were determined and docked to TftD by using Material Studio 4.4 and Discovery Studio 2.1 programs (Accelrys Software Inc.). A grid-based receptor-flexible docking module (CDOCKER) in Discovery Studio 2.1 was used for docking (*26-27*). The TftD-FADHOOH-substrate ternary complex was placed in a sphere with diameter 80 Å. Water molecules overlapping within 2.5 Å of the ternary complex were deleted. The whole system was then neutralized with seven sodium ions. After that, the system was heated from absolute zero to 298.15 K in 50 ps, and a trajectory of 500 ps was computed to reach an equilibration state (1fs/step). A 5 ns stochastic boundary molecular dynamics (SBMD) simulation with canonical ensemble (NVT, 298.15 K) was performed to mimic the aqueous environment (*28*).

Three snapshots were taken at 3 ns, 4 ns, and 5 ns of the molecular dynamics run. These structures serve as starting configurations for the following geometry optimizations and transition-state search.

2.2 QM/MM calculations

The QM/MM calculations were performed with the aid of ChemShell (*29*), which integrates Turbomole (*30*) and DL-POLY programs (*31*). Hybrid delocalized internal coordinate (HDLC) (*32*) was adopted through the calculations, and QM-region was treated by the DFT (*33*) method, while MM-region was treated by CHARMM22 force field (*34*). In the QM side, the truncated covalent bonds between the QM-region and MM-region were complemented by adding hydrogen link atoms. A charge shift model (*35*) was used to avoid over polarization of the QM density of the QM-region. Before performing QM/MM studies, some criteria were considered to guarantee the reasonability of the QM/MM partitioning: (1) residues that involved in the bond cleavage or formation should be considered in the QM region; (2) residues that strongly interact with the reactive center should also be incorporated into the QM region. As a result, the QM-region of system TftD-FADHOOH-2,4,5-TCP contains oxidation state of co-enzyme FADHOOH, residues Arg100, Phe153, Val154, Thr192, His289 and the substrate 2,4,5-TCP. This resulted in 98 QM atoms in total. The size-dependency was carefully checked by performing single-point calculations with an even larger QM region (212 atoms, details were provided in Table S1). The calculated energy barriers indicate that it is

reasonable to include 98 atoms in the QM-region. We scanned the potential energy profile along the reaction path, and the structure with the highest energy (transition state structure) was optimized by combining partitioned rational function optimizer (P-RFO) algorithm (*36*) and the low-memory Broyden-Fletcher-Goldfarb-Shanno (L-BFGS) algorithm (*37*). Harmonic vibrational frequency calculations for stationary points were performed to determine the zero-point energy (ZPE) as well as to validate the transition state character. The QM-region was optimized at the B3LYP/6-31G(d,p) level while a larger basis set, B3LYP/6-311++G(d,p), was employed in single point energy calculations. In the QM/MM calculations, both the energetic and structural contributions from the MM-region on the chemical reaction occurring at the active site were considered.

3. Results and discussion

Recent room-temperature single molecule experiments have shown that the rate constant of a single enzyme molecule is not constant but exhibits large fluctuations with a broad range (1 ms~100 s) (*38-39*). The overall rate constant k_{cat} is the integrated results by considering all the fluctuant rate constants of a single enzyme molecule (*40*). By assuming that each snapshot extracted from the dynamics trajectory corresponds to a local rate constant, many excellent QM/MM studies have shown that the calculated average barrier by Boltzmann-weighted averaging method correspond well to the overall k_{cat} (*41-42*). Thus three different snapshots extracted at 3, 4 and 5

ns from the trajectory were used as the start points in the present study. The Boltzmann-weighted average barriers were obtained by using the following equation (*43-44*):

$$\Delta E_{ea} = -RT \ln\left\{\frac{1}{n}\sum_{i=1}^{n}\exp\left(\frac{-\Delta E_i}{RT}\right)\right\} \quad (1)$$

Where, ΔE_{ea} is the average barrier, R is gas constant, n is the number of snapshots, ΔE_i is the energy barrier of path i, and T is the temperature. If not specially noted, the "average barrier" mentioned in the following paragraphs refers to Boltzmann-weighted averaging barrier. For convenience of the description, several atoms in the QM-region are numbered, as presented in Scheme 1.

3.1 Reaction mechanism and Potential energy profiles

Despite the substrate differences (2,4,5-TCP, 2,4,6-TCP, or 2,5-DiCHQ), all the degradation processes catalyzed by TftD contain two elementary steps: hydroxylation and dechlorination, as indicated in Scheme 2 and 3. The calculated energy barriers of the hydroxylation step is much higher than that of the dechlorination step, which implies that hydroxylation is the rate-determining step during the catalytic processes of TftD toward these poly-CPs (Figure 1). A substantial energy barrier spread for this step has been found during the degradation process of 2,4,5-TCP (16.3~24.7 kcal mol^{-1}) among different snapshots. Similar energy barrier spreads for 2,4,6-TCP (17.8~23.1 kcal mol^{-1}) and 2,5-DiCHQ (19.7~27.8 kcal mol^{-1}) were also found. These observed energy barrier fluctuations may be helpful in understanding the recent single molecule experimental evidences

that the reaction rate of a single enzyme molecule exhibits large fluctuations (*38, 39*). In addition, the calculated average barriers for the hydroxylation step of 2,4,5-TCP, 2,4,6-TCP, and 2,5-DiCHQ are 16.9, 18.4, 19.7 kcal mol^{-1}, correspond well with the experimentally determined overall k_{cat} values (0.67 s^{-1}, 0.41 s^{-1}, and 0.10 s^{-1}) (*17, 19*).

The calculated energy barriers for the dechlorination steps are relatively low (0.3, 0.2, 0.2 kcal mol^{-1}). This implies that the hydroxylated substrate (like IM3, hydroxylated 2,4,5-TCP) is unstable and can be quickly transformed to the product (like P-5, 2,5-DiCBQ) by TftD. To verify this conclusion, the QM only calculations of the QM-region were also performed. The energy barriers for the dechlorination steps of 2,4,5-TCP, 2,4,6-TCP, and 2,5-DiCHQ are 2.9, 3.5, and 1.1 kcal/mol, which also indicates the low barrier character of the dechlorination steps. The reaction heats for all the dechlorination pathways range from -38.5 to -29.8 kcal mol^{-1}, indicating that the degradation processes toward 2,4,5-TCP, 2,4,6-TCP, and 2,5-DiCHQ are irreversible. It is worth mentioning that the experimentally detected degradation products (5-Cl-2-H-BQ) of 2,5-DiCHQ is not P10 (4-chloro-3-hydroxy-benzoquinone, 4-Cl-3-H-BQ) shown in Scheme 3. The spatial locations of active site residues in TftD do not favor the transformation of 4-Cl-3-H-BQ to 5-Cl-2-H-BQ. Thus, 4-Cl-3-H-BQ might be spontaneously isomerized to 5-Cl-2-H-BQ in the solution, as indicated by the fact that the energy of 5-Cl-2-H-BQ is about 10.4 kacl mol^{-1} lower than that of 4-Cl-3-H-BQ (Figure S1). In the solution, 5-Cl-2-H-BQ can then be further transformed to 5-Cl-2-H-HQ by nicotinamide adenine dinucleotide (NADH).

3.2 Catalytic Itinerary and Structural Details

Since a majority of the catalytic reactions proceed through pathways with the highest reaction rates, the following investigations will mainly focus on pathways with the lowest energy barriers during the degradation processes toward 2,4,5-TCP, 2,4,6-TCP, and 2,5-DiCHQ, respectively. Table 1 shows the natural bond orbital (NBO) charges of some groups (O_dH_d, O_dH_d-adduct, $FADHO_pO_dH_d$) calculated at B3LYP/6-31G(d,p)//CHARMM22 level as well as some key bond lengths (O_p-O_d, O_d-C_4, C_4-Cl_d and O_a-H_a) obtained at the B3LYP/6-31G(d,p)//CHARMM22 level. For a more intuitive observation, the three dimension structures of R-1, TS-2, and IM-3 involved in the hydroxylation step (rate-determining) of 2,4,5-TCP were provided in Figure 2. Structures of R'-1, TS'-2, IM'-3, R-6, TS-7, and IM-8 involved in the hydroxylation step (rate-determining) of 2,4,6-TCP and 2,5-DiCHQ were provided in Figure S2 and S3. Take substrate 2,4,5-TCP as an example, the hydroxylation process (R1→TS-2→IM-3) are mainly indicated by the variations of bonds O_p-O_d and O_d-C_4. The length of bond O_p-O_d varies from 1.45 to 1.89 and 2.78 Å while O_d-C_4 changes from 3.88 to 1.97 and 1.39 Å. Two hydrogen bonds (H_b-O_p and H_b-O_d) were found in the R-1, TS-2, and IM-3 structures, highlighting the role of a previously unnoticed residue Arg100. Detailed analysis shows that both of the hydrogen bonds in TS-2 (2.20 and 2.73 Å) are stronger than in R-1 (2.51 and 3.54 Å), which implies a positive role of Arg100 during the hydroxylation step. Similar roles during the hydroxylation step of 2,4,6-TCP and 2,5-DiCHQ were also found (Table 1). The length of bond C_4-Cl_d changes from 1.80 Å (IM-3), 1.91 Å (TS-4) to 3.26 Å (P-5) during the dechlorination process, indicating the formation of a chloride ion. The anion character

of Cl_d in the product was confirmed by its negative charge (Cl_d, -0.75).

During the degradation processes toward 2,4,5-TCP, 2,4,6-TCP, and 2, 5-DiCHQ, the calculated NBO charges of the O_dH_d group are -0.11, -0.10, and -0.11, respectively. This near radical character of O_dH_d has been proposed in other $FADH_2$-dependent enzymes like p-hydroxybenzoate hydroxylase (*45*), which seemingly challenges the OH cation transfer mechanism established in another study on p-hydroxybenzoate hydroxylase (*46*). However, no radicals were found in IM-3 in the present study, as indicated by the negatively charged $FADHO_d^-$ (-0.88, -0.86, and -0.84) and neutral character of OH-adduct (0.00, 0.01, and 0.07). Direct comparison of the co-enzyme in R-1 ($FADHO_pO_dH_d$) and IM-3 ($FADHO_d^-$) implies that the co-enzyme acquired an electron after hydroxylation process through heterolysis rather than hemolysis of the O_d-O_p bond. The observed O_dH_d radical only exits in structure TS-2 during this hydroxylation (single electron transfer) process.

3.3 Individual Residue Influence and substrate selectivity

The electrostatic influence of ten residues toward the hydroxylation processes of 2,4,5-TCP, 2,4,5-TCP, and 2,5-DiCHQ were estimated. The activation energy difference caused by amino acid i can be described as:

$$\Delta E^{i-0} = \Delta E^{i} - \Delta E^{0}$$

Where ΔE^{i-0} is the changes of the barrier, ΔE^{i} is the energy barrier with charges on residue i set to 0, and ΔE^{0} is the original values of the energy barrier. The geometry structures of the stationary points were kept unchanged during all these calculations.

A positive ΔE^{i-0} value means that the ith residue lowers the energy barrier and facilities the catalytic reaction. The ΔE^{i-0} values of eleven residues were schematically represented in Figure 3. The electrostatic influences of the ten studied residues toward substrate 2,4,5-TCP and 2,4,6-TCP are similar. Glu251 and Arg366 significantly suppress the hydroxylation processes of 2,4,5-TCP by increasing the reaction barrier of about 9.1 and 7.4 kcal mol^{-1} (ΔE^{i-0} = -7.4 kcal/mol) while they suppress the hydroxylation processes of 2,4,6-TCP by increasing the reaction barrier of about 9.9 and 8.8 kcal mol^{-1}. All the other studied residues have a relative weaker influence towards the hydroxylation processes (-2.0 kcal/mol < ΔE^{i-0} < 2.0 kcal/mol). Our electrostatic influence analysis highlights Glu251 and Arg366 as candidate residues for future mutation studies.

The reason why TftD can catalyze 2,5-DiCHQ but not 2,6-DiCHQ stays unclear. Since the degradation sites of substrates 2,4,5-TCP, 2,4,6-TCP, 2,5-DiCHQ, and PCP are all found at 3, 4, or 5-positions but not at 2, or 6-positions, it has been proposed that the spatial locations of substrates may significantly influence the degradation process (*14-15, 17, 19*). Like the other poly-CPs, the most favorable locations of 2,6-DiCHQ are the 3,5-positions (with no chlorine atoms) ready to be hydroxylated. The energies of unfavorable locations of 2,6-DiCHQ (2,6-positions ready to be hydroxylated, named as 2,6-DiCHQ') are about 11.5 kcal mol^{-1} higher than the favorable locations calculated at B3LYP/6-311++G(d,p)//CHARMM22 level. Further QM/MM hydroxylation calculations on the 6-position of 2,6-DiCHQ' shows a comparable hydroxylation energy barrier (22.7 kcal mol^{-1}) with

TftD-FAD$O_pO_dH_d$-2,5-DiCHQ complex (20.4 kcal mol^{-1}). The transition state character was also confirmed by the imaginary frequency (321.5i). As a result, for hydroxylation of 2,6-DiCHQ, an extremely high barrier of ~34.2 (11.5 plus 22.7) kcal mol^{-1} should be crossed. These results show that spatial locations of 2,6-DiCHQ as well as the hydroxylation barrier are the two possible reasons why 2,6-DiCHQ cannot be further degraded by TftD.

4. Conclusions

In the present work, the degradation processes of enzyme TftD towards substrates 2,4,5-TCP, 2,4,6-TCP, and 2,5-DiCHQ were calculated by using QM/MM method. Two elementary steps (hydroxylation and dechlorination) were found during the degradation processes for all the three substrates. The hydroxylation step was found to be rate-determining step with average barriers 16.3, 17.8, and 19.7 kcal mol^{-1} for 2,4,5-TCP, 2,4,6-TCP, and 2,5-DiCHQ, respectively. Substantial energy barrier spreads on the hydroxylation steps have been found, in agreement with the previous room-temperature single molecule experiments (reaction rate varies among different enzymatic conformations). In addition, electrostatic influences of individual neighboring residues on hydroxylation steps were analyzed and residues Glu251 and Arg366 were highlighted as candidate residues for future mutation studies. Moreover, we have shown that spatial locations of 2,6-DiCHQ as well as the hydroxylation barrier are the two possible reasons why 2,6-DiCHQ cannot be further degraded by TftD.

Acknowledgements

The work was financially supported by NSFC (National Natural Science Foundation of China, project Nos. 21337001, 21377073 and 21177076) and Taishan Grand (No. ts20120522).

Supplementary Information

Table S1 Dependency of the energy barriers on the QM size, the smaller QM region (98 atoms) contains oxidation state of co-enzyme FADHOOH, functional groups of residues Arg100, Phe153, Val154, Thr192, His289 and the substrate 2,4,5-TCP, the larger QM region (212 atoms) contains additional residues such as Ala104, Pro150, Leu151, Glu251, Phe285, Cal288, Arg295, Arg366, and Phe442. **Figure S1** The optimized structures and calculated energies of 5-Cl-2-H-BQ and 4-Cl-3-H-BQ (P-10). **Figure S2** Optimized reactant (R'-1), transition state (TS'-2), and intermediate (IM'-3) structures for the hydroxylation step of TftD towards 2,4,6-TCP. The unit of the bond distances and imaginary frequency are in Å and cm^{-1}. **Figure S3** Optimized reactant (R-6), transition state (TS-7), and intermediate (IM-8) structures for the hydroxylation step of TftD towards 2,5-DiCHQ. The unit of the bond distances and imaginary frequency are in Å and cm^{-1}.

References

1 A. O. Olaniran, and E. O. Igbinosa, *Chemosphere*, 2011, **83**, 1297–1306.

2 L. Y. Xun, and C. M. Webster, *J. Biol. Chem.*, 2004, **297**, (8), 6696–6700.

3 D. G. Crosby, *Pure Appl. Chem.*, 1981, **53**, 1052–1080.

4 D. Firestone, *Stockh. Ecol. Bull.*, 1978, **27**, 39–52.

5 E. Hoekstra, H. de Weerd, E. de Leer, and U. Brinkman, *Environ. Sci. Technol.*, 1999, **33**, 2543–2549.

6 I. P. Solyanikova, and L. A. Golovleva, *J. Environ. Sci. Health. B*, 2004, **39**, 333–351.

7 J. A. Field, and R. Sierra-Alvarez, *Rev. Environ. Sci. Biotechnol.*, 2008, **7**, 211–241.

8 P. K. Arora1 and H. Bae, *Microb. Cell Fact*., 2014, **13**, 31.

9 M. Tarao, and M. Seto, *Appl. Environ. Microbiol.*, 2000, **66**, 566–570.

10 M. Goswami, N. Shivaraman, R. P. Singh, *World J. Microbiol. Biotechnol.*, 2002, **18**, 779–783.

11 J. S. Uotila, M. S. Salkinoja-Salonen, and J. H. A. Apajalahti, *Biodegradation*, 1991, **2**, 25–31.

12 S. Kellogg, D. Chatterjee, and A. Chakrabarty, *Science*, 1981, **214**, 1133–1135.

13 H. Koike, H. Sasaki, T. Kobori, S. Zenno, K. Saigo, M. E. Murphy, E. T. Adman, and M. Tanokura, *J. Mol. Biol.*, 1998, **280**, 259–273.

14 G. Martin, I. Artaud, and C. Capeillère-Blandin, *Biochim. Biophys. Acta.*, 2001, **1547**, 288–301.

15 G. Martin, S. Dijols, C. Capeillere-Blandin, and I. Artaud, *Eur. J. Biochem.*, 1999,

261, 533–539.

16 L. Y. Xun, *J. Bacteriol.*, 1996, **178**, 2645–2649.

17 M. R. Gisi, and L. Y. Xun, *J. Bacteriol.*, 2003, **185**, 2786–2792.

18 A. Hubner, C. E. Danganan, L. Y. Xun, A. M. Chakrabarty, and W. Hendrickson, *Appl. Environ. Microb.*, 1998, **64**, 2086–2093.

19 B. N. Webb, J. W. Ballinger, E. Kim, S. M. Belchik, K. S. Lam, B. Youn, M. S. Nissen, L. Y. Xun, and C. Kang, *J. Biol. Chem.*, 2010, **285**, 2014–2027.

20 W. Thiel, and G. Hummer, *Nature*, 2013, **504**, 96–97.

21 G. Ma, L. Dong, and Y. Liu, *RSC Adv.*, 2014, **4**, 35449-35458.

22 C. Li, and S. Shaik, *RSC Adv.*, 2013, **3**, 2995-3005.

23 H. Li, A. D. Robertson, and J. H. Jensen, *Proteins*, 2005, **61**, 704–721.

24 B. R. Brooks, R. E. Bruccoleri, B. D. Olafson, D. J. States, S. Swaminathan, and M. Karplus, *J. Comput. Chem.*, 1983, **4**, 187–217.

25 B. R. Brooks, C. L. Brooks III, A.D. Mackerell, L. Nilsson, R. J. Petrella, B. Roux, Y. Won, G. Archontis, C. Bartels, S. Boresch, A. Caflisch, L. Caves, Q. Cui, A. R. Dinner, M. Feig, S. Fischer, J. Gao, M. Hodoscek, W. Im, K. Kuczera, T. Lazaridis, J. Ma, V. Ovchinnikov, E. Paci, R. W. Pastor, C. B. Post, J. Z. Pu, M. Schaefer, B. Tidor, R. M. Venable, H. L. Woodcock, X. Wu, W. Yang, D. M. York, and M. Karplus, *J. Comp. Chem.*, 2009, **30**, 1545–1615.

26 G. Wu, D. H. Robertson, C. L. Brooks III, and M. Vieth, *J. Comput. Chem.*, 2003, **24**, 1549–1562.

27 M. Vieth, J. D. Hirst, A. Kolinski, and C. L. Brooks III, *J. Comput. Chem.*, 1998,

19, 1612–1622.

28 C. L. Brooks, and M. Karplus, *J. Chem. Phys.*, 1983, **79**, 6312–6325.

29 P. Sherwood, A. H. D. Vries, M. F. Guest, G. Schreckenbach, C. R. A. Catlow, S. A. French, A. A. Sokol, S. T. Bromley, W. Thiel, A. J. Turner, S. Billeter, F. Terstegen, S. Thiel, J. Kendrick, S. C. Rogers, J. Casci, M. Watson, F. King, E. Karlsen, M. Sjovoll, A. Fahmi, A. Schafer, and C. Lennartz, *J. Mol. Struc-Theochem.*, 2003, **632**, 1–28.

30 R. Ahlrichs, M. Bär, M. Häser, H. Horn, and C. Kölmel, *Chem. Phys. Lett.*, 1989, **162**, 165–169.

31 W. Smith, and T. R. Forester, *J. Mol. Graphics.*, 1996, **14**, 136–141.

32 S. R. Billeter, A. J. Turner, and W. Thiel, *Phys. Chem. Chem. Phys.*, 2000, **2**, 2177–2186.

33 K. Burke, J. Werschnik, and E. K. U. Gross, *J. Chem. Phys*., 2005, **123**, 62206.

34 A. D. MacKerell, D. Bashford, M. Bellott, R. L. Dunbrack, J. D. Evanseck, M. J. Field, J. Gao, H. Guo, S. Ha, D. Joseph-McCarthy, L. Kuchnir, K. Kuczera, F. T. K. Lau, C. Mattos, S. Michnick, T. Ngo, D. T. Nguyen, B. Prodhom, W. E. Reiher, B. Roux III, M. Schlenkrich, J. C. Smith,; R. Stote,; J. Straub, M. Watanabe, J. Wiórkiewicz-Kuczera, D. Yin, and M. Karplus, *J. Phys. Chem. B*, 1998, **102**, 3586–3616.

35 A. H. de Vries, P. Sherwood, S. J. Collins, A. M. Rigby, M. Rigutto, and G. J. Kramer, *J. Phys. Chem. B*, 1999, **103**, 6133–6141.

36 J. Baker, *J. Comput. Chem.*, 1986, **7**, 385–395.

37 D. C. Liu, and J. Nocedal, *Math. Program.*, 1989, **45**, 503–528.

38 H. P. Lu, L. Xun, and X. S. Xie, *Science*, 1998, **282**, 1877–1882.

39 W. Min, B. P. English, G. Luo, B. J. Cherayil, S. C. Kou, and X. S. Xie, *Acc. Chem. Res.*, 2005, **38**, 923–931.

40 X. S. Xie, *Science*, 2013, **342**, 1457–1459.

41 P. Saura, R. Suardíaz, L. Masgrau, J. M. Lluch, and À. González-Lafont, *ACS Catal.*, 2014, **4**, 4351–4363.

42 R. Lonsdale, K. T. Houghton, J. Żurek, C. M. Bathelt, N. Foloppe, M. J. de Groot, J. N. Harvey, and A. J. Mulholland. *J. Am. Chem. Soc.*, 2013, **135**, 8001-8015.

43 R. Lonsdale, J. N. Harvey, A. and J. Mulholland, *J. Phys. Chem. B*, 2010, **114**, 1156–1162.

44 Y. Li, X. Shi, Q. Zhang, J. Hu, J. Chen, and W. Wang, *Environ. Sci. Technol.*, 2014, **48**, 5008-5016.

45 R. D. Bach, *J. Phys. Chem. A*, 2011, **115**, 11087–11100.

46 M. Ortiz-Maldonado, D. P. Ballou, and V. Massey, *Biochemistry*, 1999, **38**, 8124–8137.

Table 1 Calculated key group charges (O_dH_d, O_dH_d-adduct, and $FADHO_pO_dH_d$) at the B3LYP/6-311++G(d,p)//CHARMM22 level and key lengths of bonds (O_p-O_d, O_d-C_4, C_4-Cl_d and O_a-H_a) at the B3LYP/6-31G(d,p)//CHARMM22 level during the degradation processes toward 2,4,5-TCP, 2,4,6-TCP, and 2,5-DiCHQ.

Substrates	Structures	Bonds/(Å)					Charges/(e)		
		O_p-O_d	O_d-C_4	C_4-Cl_d	H_b-O_p	H_b-O_d	O_dH_d	O_dH_d-adduct	$FADHO_pO_dH_d$
	R-1	1.45	3.88	1.73	2.51	3.54	0.05	-	0.00
	TS-2	1.89	1.97	1.76	2.20	2.73	-0.11	-	-0.48
2,4,5-TCP	IM-3	2.78	1.39	1.80	1.73	3.56	-0.17	0.00	-1.05
	TS-4	2.70	1.32	1.91	1.85	3.56	-	-	-
	P-5	2.79	1.23	3.26	2.96	2.35	-	-	-
	R'-1	1.45	3.75	1.74	2.43	3.42	0.05	-	0.01
	TS'-2	1.90	1.94	1.76	2.19	2.63	-0.10	-	-0.47
2,4,6-TCP	IM'-3	2.86	1.40	1.81	1.80	4.19	-0.17	0.01	-1.03
	TS'-4	2.86	1.37	1.89	1.79	4.16	-	-	-
	P'-5	2.87	1.23	3.26	3.18	1.99	-	-	-
	R-6	1.45	2.75	1.75	1.98	2.39	0.05	-	0.04
	TS-7	1.95	1.91	1.75	1.79	2.53	-0.11	-	-1.54
2,5-DiCHQ	IM-8	2.89	1.4	1.82	1.64	4.07	-0.24	0.07	-1.08
	TS-9	2.43	1.36	1.86	1.76	3.68	-	-	-
	P-10	3.25	1.24	2.93	2.52	3.89	-	-	-

Figure Captions

Scheme 1 Arrangement of active site. The boundary between the QM and MM region is indicated by wavy lines.

Scheme 2 TftD catalyzed degradation reactions from 2,4,5-TCP to 2,5-DiCHQ.

Scheme 3 TftD catalyzed degradation reactions from 2,5-DiCHQ to 5-Cl-2-H-HQ.

Figure 1 Energy profile of TftD catalyzed degradation reactions toward 2,4,5-TCP (red), 2,4,6-TCP (blue), and 2,5-DiCHQ at the B3LYP/6-311++G(d,p)//CHARMM22 level. The lowest hydroxylation barriers for the three substrates are indicated by bold lines and numbers while the numbers in the braces are the calculated Boltzmann-weighted average barriers.

Figure 2 Optimized reactant (R-1), transition state (TS-2), and intermediate (IM-3) structures for the hydroxylation step of TftD towards 2,4,5-TCP at B3LYP/6-31G(d,p)//CHARMM22 level. The unit of the bond distances and imaginary frequency are in Å and cm^{-1}.

Figure 3 ΔE^{i-0} values of ten individual residues toward the hydroxylation step of 2,4,5-TCP, 2,4,6-TCP, and 2,5-DiCHQ.

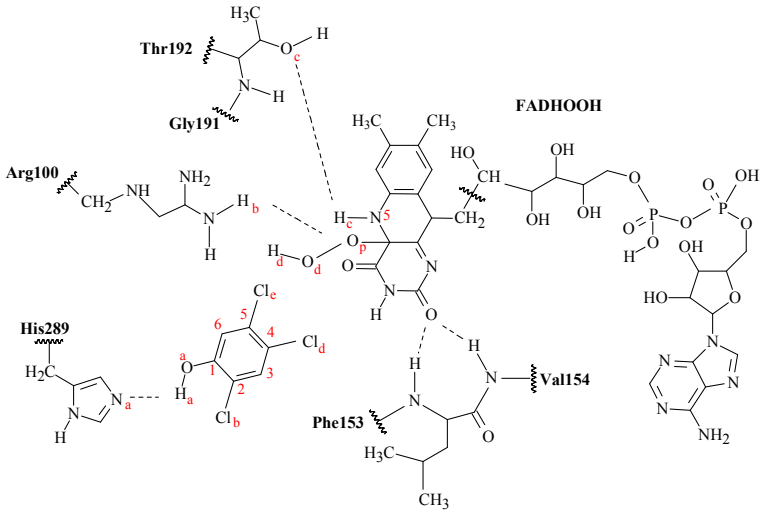

Scheme 1

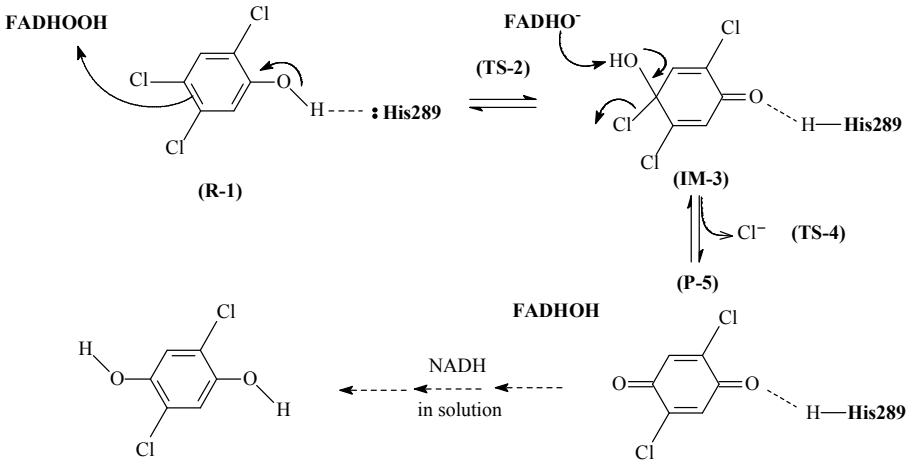

Scheme 2

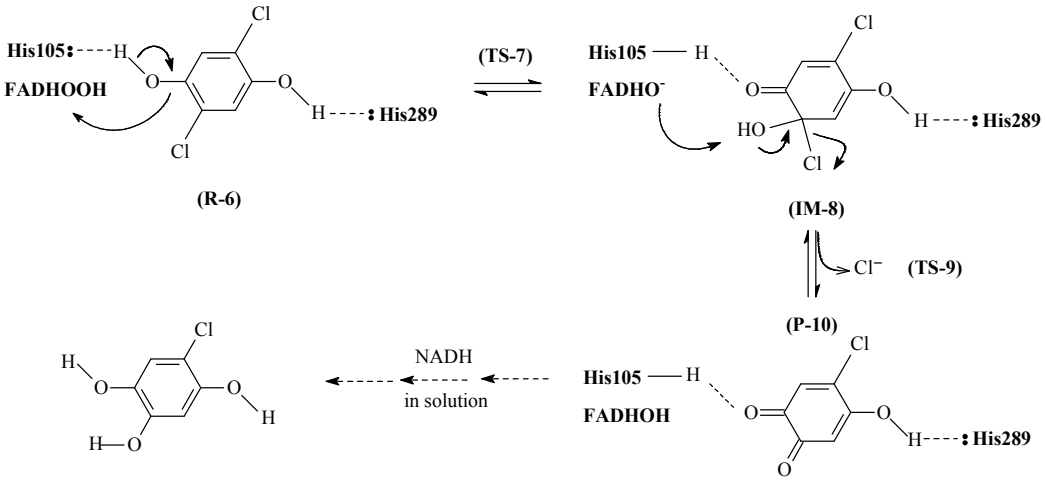

Scheme 3

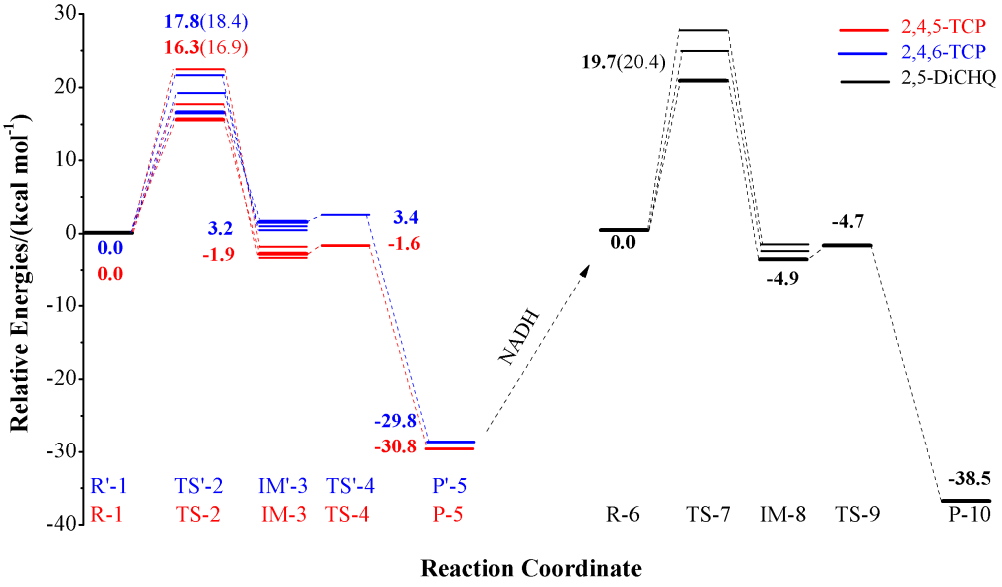

Figure 1

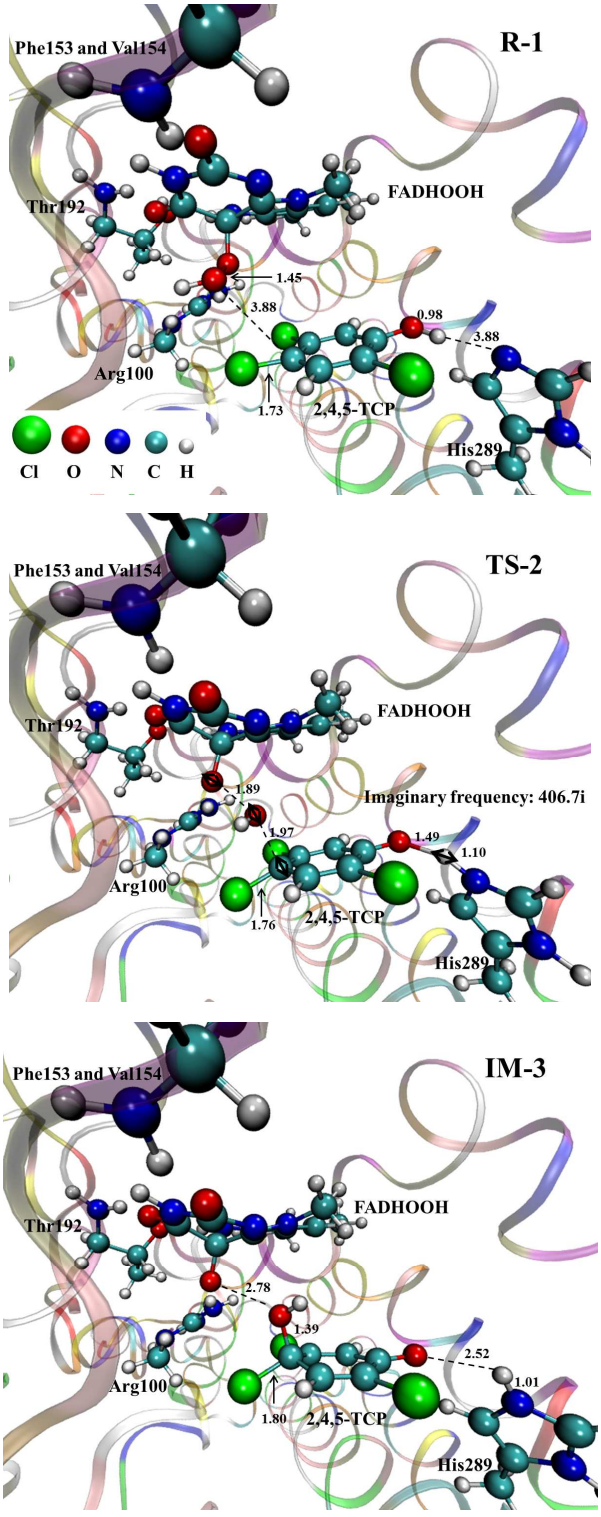

Figure 2

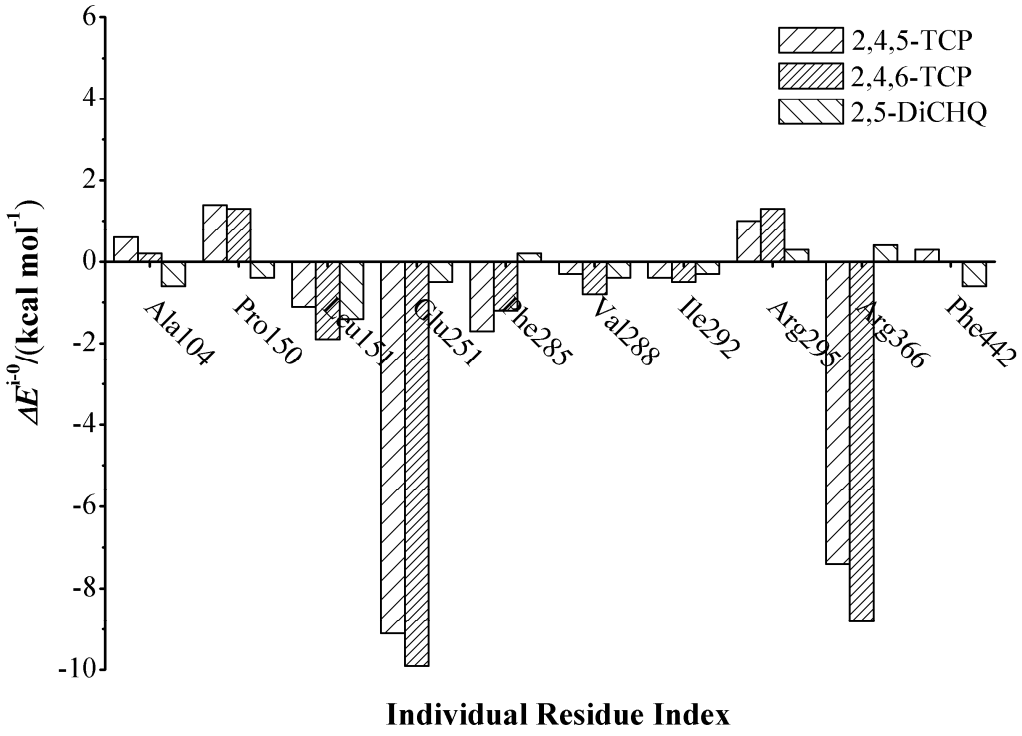

Figure 3